Two-Photon Fluorescence Imaging and Bimodal Phototherapy of Epidermal Cancer Cells with Biocompatible Self-Assembled Polymer Nanoparticles

ARTICLE *in* BIOMACROMOLECULES · MARCH 2014

Impact Factor: 5.75 · DOI: 10.1021/bm500156z · Source: PubMed

6 AUTHORS, INCLUDING:

Noufal Kandoth
U. Pavia; ISOF-CNR, Bologna, Italy
16 PUBLICATIONS **189** CITATIONS
SEE PROFILE

Vladimir Kirejev
University of Gothenburg
9 PUBLICATIONS **44** CITATIONS
SEE PROFILE

Ruxandra Gref
Université Paris-Sud 11
148 PUBLICATIONS **9,722** CITATIONS
SEE PROFILE

Salvatore Sortino
University of Catania
185 PUBLICATIONS **3,383** CITATIONS
SEE PROFILE

Article

Two-Photon-Fluorescence Imaging and Bimodal Phototherapy of Epidermal Cancer Cells with Biocompatible Self-Assembled Polymer Nanoparticles

Noufal Kandoth, Vladimir Kirejev, Sandra Monti, Ruxandra Gref, Marica B Ericson, and Salvatore Sortino

Biomacromolecules, **Just Accepted Manuscript** • DOI: 10.1021/bm500156z • Publication Date (Web): 27 Mar 2014

Biomacromolecules

Two-Photon-Fluorescence Imaging and Bimodal Phototherapy of Epidermal Cancer Cells with Biocompatible Self-Assembled Polymer Nanoparticles

Noufal Kandoth,[†] Vladimir Kirejev,[§] Sandra Monti,[‡] Ruxandra Gref,[¥] Marica B. Ericson,[§] and Salvatore Sortino[†,*]

Laboratory of Photochemistry, Department of Drug Sciences, University of Catania, Viale Andrea Doria 6, I-95125 Catania, Italy; Biomedical Photonics Group, Department of Chemistry and Molecular Biology, University of Gothenburg, Kemivägen 10, SE 412 96, Sweden; Istituto per la Sintesi Organica e la Fotoreattività-CNR, I-40129, Bologna, Italy; UMR CNRS 8612, Faculty of Pharmacy, Paris Sud University, 92290 Châtenay-Malabry, France

E-Mail: ssortino@unict.it

Abstract: We have developed herein an engineered polymer-based nanoplatform showing the convergence of two-photon fluorescence imaging and bimodal phototherapeutic activity in a single nanostructure. It was achieved through the appropriate choice of three different components: a β-cyclodextrin-based polymer acting as a suitable carrier, a zinc phthalocyanine emitting red fluorescence simultaneously as being a singlet oxygen ($^1O_2$) photosensitizer, and a tailored nitroaniline derivative, functioning as a nitric oxide (NO)

† University of Catania
§ University of Gothenburg
‡ ISOF-CNR Bologna
¥ CNRS, Paris Sud University

photodonor. The self-assembly of these components results in photoactivable nanoparticles, approximately 35 nm in diameter, co-encapsulating a multifunctional cargo, which can be delivered to carcinoma cells. The combination of steady-state and time-resolved spectroscopic and photochemical techniques shows that the two photoresponsive guests do not interfere with each other while being enclosed in their supramolecular container and can thus be operated in parallel under control of light stimuli. Specifically, two-photon fluorescence microscopy allows mapping of the nanoassembly, here applied to epidermal cancer cells. By detecting the red emission from the phthalocyanine fluorophore it was also possible to investigate the tissue distribution after topical delivery onto human skin *ex vivo*. Irradiation of the nanoassembly with visible light triggers the simultaneous delivery of cytotoxic $^1O_2$ and NO, resulting in an amplified cell photomortality due to a combinatory effect of the two cytotoxic agents. The potential of dual therapeutic photodynamic action and two-photon fluorescence imaging capability in a single nanostructure make this system an appealing candidate for further studies in biomedical research.

Keywords: Phototherapy, Two-Photon Fluorescence, Self-Assembly, Polymer Nanocarriers

Introduction

The release of multiple therapeutic agents in a controlled fashion is a challenging goal in view of multimodal therapy applications. These emerging treatment modalities exploit either additive or synergistic effects of different biologically active species, preferably generated at the same cellular site, with the final goal of maximizing the therapeutic efficacy and minimizing side effects.[1] In this frame, light represents a powerful tool to trigger rapid introduction of the therapeutic agents at the target site with exquisite control of localization, timing and dosage, three of the main factors responsible for the therapeutic outcome.[2] In addition, light-triggering is "bio-friendly", providing fast reaction rates, and offering the great benefit of not affecting physiological values of temperature, pH and ionic strength, fundamental requisite for biomedical applications. These properties make the phototherapeutic methods a powerful arsenal in the burgeoning field of nanomedicine with intriguing potential to tackle cancer diseases in a noninvasive way.[3]

Singlet oxygen ($^1O_2$) and nitric oxide (NO) represents two of the main cytotoxic species that can be produced upon light excitation of suitable photosensitizers.[4,5] In particular, $^1O_2$ is the actual active agent in photodynamic therapy (PDT)[4a-c] and is photogenerated by energy transfer between the lowest triplet state of photosensitizers such as porphyrins or phthalocyanines, and molecular oxygen.[4d] NO has recently come to the limelight not only for its pivotal role in the maintenance and regulation of vital cell functions[6] but also for its promising anticancer activity.[7] $^1O_2$ and NO share several important features such as: i) small size and absence of charge, ii) capability to attack biological substrates of different nature (*i.e.,* lipids, proteins, and DNA), iii) absence of multidrug resistance, a major factor in the failure of many forms of chemotherapy, iv) confinement of their action to short distances from production site inside the cells (< 20 nm for $^1O_2$ and < 200 μm for NO), due to their short lifetime, reducing systemic toxicity issues common to many conventional drugs. In addition, since NO photorelease is independent from O_2 availability, it very well complements PDT at the onset of hypoxic conditions, typical for some tumors, where PDT may fail. On these grounds the fabrication of multifunctional nanoconstructs enabling simultaneous release of $^1O_2$ and NO and, at the same time, tracing in a cellular environment *via* fluorescence techniques, represents in principle an ideal strategy in view of "image-guided" bimodal phototherapy. At this regard, two-photon excitation (TPE) with near infrared (NIR) light in the range of about 700-1000 nm is less detrimental to healthy cells and has a deeper penetration through tissue due to a reduced absorption and scattering by water and biological substances. Therefore, TPE fluorescence microscopy represents a valuable tool in biosciences.[8] Furthermore, given the intrinsic localization of the excitation process due to its non-linear properties, TPE can provide additional spatial resolution, since excitation occurs primarily at the focal point of the light source.

Polymer nanocarriers are promising vehicles for the delivery of drugs through the blood stream to target locations in living organisms.[9] In particular, hydrosoluble polymers able to assemble spontaneously into particles of nanoscaled dimensions represent invaluable supramolecular scaffolds for the realization of multifunctional and photoresponsive nanoconstructs for a diversity of biomedical applications.[10] Multiple photoresponsive character can be imposed to nanoparticles (NPs) based on the assembly of two different polymers with the covalent introduction of appropriate chromophores in the individual macromolecular components.[11] Alternatively, photoresponsive chromophores with distinct functions can be noncovalently co-encapsulated in the hydrophobic interior of the NPs to ensure multifunctional character in a confined region of space.[12] Focusing on solubility and aggregation issues in aqueous medium, cyclodextrin (CD) polymers offer the possibility of guest interaction with diverse binding sites, *i.e.* within the 3D macromolecular network and the CD cavities, thereby enhancing the apparent solubility and regulating the self-association tendency of drugs.[13] For example, an epichlorohydrin crosslinked β-CD polymer of high molecular weight, spontaneously forming NPs in water, is able to effectively monomerize doxorubicin.[14] Furthermore, we have recently demonstrated that the same β-CD polymer can be made photoresponsive and useful for both imaging and therapy upon co-encapsulation of suitable chromophoric components.[15] In this frame, we report herein the design, preparation, spectroscopic and photochemical characterization of a further multifunctional photoactivable nanoplatform based on the epichlorohydrin-β-CD copolymer, combining phototherapeutic activity and applicability for imaging by two-photon fluorescence microscopy. This type of multifunctionality represent a great advantage for image-guided phototherapy. A proof-of-principle demonstration of the biological applications of the system is offered. The functionalized NPs are obtained *via* self-assembling of three *ad-hoc* chosen components: i) the epichlorohydrin-β-CD copolymer **1** as suitable carrier, ii) the zinc

phthalocyanine **2** as red-absorbing fluorophore suitable for two-photon excitation and simultaneously acting as a $^1O_2$ photosensitizer, and iii) the tailored molecular conjugate **3** as NO photodonor (Scheme 1). We demonstrate that this polymeric nanoplatform i) can be localized in human epidermal cancer cells by two-photon fluorescence microscopy, ii) simultaneously releases $^1O_2$ and NO under visible light illumination and, as a consequence, iii) induces amplified cancer cell mortality due to bimodal phototherapeutic activity.

Experimental Section

Chemicals. Poly-β-CD polymer **1** was prepared by crosslinking β-CD with epichlorohydrin (EP), under strong alkaline conditions, following a described method.[13a-c] A mixture of different molecular weight compounds was obtained in the polycondensation reaction. Separation was performed with size exclusion chromatography (SEC) with water compatible high performance columns using pullulan standards. The β-CD content in **1** was 70% w/w, as determined on the basis of the ^{1}H NMR spectra from the integrated peaks of anomeric protons near 5 ppm and the integrated signals between 3 and 4 ppm due to the hydrogen atoms of the pyranose rings and of the 2-hydroxypropyl ether segment.[13a-c] The average molar mass of **1** polymer was 7×10^5 g/mol, as determined by size exclusion chromatography using pullulan standards. The macrocyclic zinc phthalocyaninetetrasulfonate **2** was purchased from Porphyrin Pdts and used without further purification. The tailored NO photodonor **3** was synthesized according to our recently reported procedures.[16] All other reagents were of highest commercial grade available and used without further purification. All solvent used (from Carlo Erba) were analytical grade.

Sample preparation. Solution of **1** was prepared by stirring overnight 8 mg mL^{-1} of **1** in PBS at pH 7.4. Compounds **2** and **3** were dissolved in methanol and slowly evaporated to

form a thin film. These films were then hydrated with an aqueous solution of **1** in PBS at a pH of 7.4. The mixtures were stirred for 5 hours at 40 °C and then the final solutions were left to equilibrate at room temperature and filtered. The polydispersity index of the NPs was *ca.* 0.15. For the binding studies, an aqueous solution of compound **2** was prepared at micromolar concentration. The inclusion behaviour of **2** with the carrier **1** was studied by adding different weighed amounts of the corresponding polymer to the aqueous solution of **2**.

Instrumentation. *Steady-state absorption, emission, photolysis and nanoparticle sizes.* UV/Vis absorption and fluorescence spectra were recorded with a thermostated HP-8452 diode array spectrophotometer and Fluorolog-2 (Model, F-111) spectrofluorimeter respectively. Photolysis experiments were performed in a thermostated quartz cell (1 cm path length, 3 mL capacity) by using a Rayonet photochemical reactor equipped with 8 RPR lamps with an emission in the 380-480 nm ranges with a maximum at 420 nm in the presence of a 400 nm cut-off filter. The incident photon flux on quartz cuvettes was *ca.* 0.8×10^{15} quanta sec^{-1}. Nanoparticle sizes were measured by a dynamic light scattering Horiba LS 550 apparatus equipped with a diode laser with a wavelength of 650 nm.

*Laser flash photolysis***.** All of the samples were excited with the second harmonic of Nd–YAG Continuum Surelite II–10 laser (532 nm, 6 ns FWHM), using quartz cells with a path length of 1.0 cm. The excited solutions were analyzed with a Luzchem Research mLFP–111 apparatus with an orthogonal pump/probe configuration. The probe source was a ceramic xenon lamp coupled to quartz fiber-optic cables. The laser pulse and the mLFP–111 system were synchronized by a Tektronix TDS 3032 digitizer, operating in pre-trigger mode. The signals from a compact Hamamatsu photomultiplier were initially captured by the digitizer and then transferred to a personal computer, controlled by Luzchem Research software operating in the National Instruments LabView 5.1 environment. The solutions were deoxygenated by bubbling with a vigorous and constant flux of pure argon (previously saturated with solvent). In all of these experiments, the solutions were renewed after each laser shot (in a flow cell of 1 cm optical path), to prevent probable auto-oxidation processes.

The sample temperature was 295 ± 2 K. The energy of the laser pulse was measured at each shot with a SPHD25 Scientech pyroelectric meter.

Singlet oxygen detection. Photogeneration of $^1O_2$ upon laser excitation of the photosensitizer was monitored by luminescence measurements in oxygen-saturated solutions. The near-IR luminescence of singlet oxygen at 1.27 μm resulting from the forbidden transition $^3\Sigma_g^- \leftarrow {}^1\Delta_g$; this was probed orthogonally to the exciting beam with a pre-amplified (low impedance) Ge-photodiode (Hamamatsu EI-P, 300 ns resolution) maintained at –196°C and coupled to a long-pass silicon filter (>1.1 μm) and an interference filter (1.27 μm). Pure signal of $^1O_2$ were obtained as difference between signals in air- and Ar-saturated solutions. The temporal profile of the luminescence was fitted to a single-exponential decay function with the exclusion of the initial portion of the plot, which was affected by scattered excitation light, fluorescence, and the formation profile of singlet oxygen itself.

Nitric oxide detection. NO release was measured with a World Precision Instrument, ISO-NO meter, equipped with a data acquisition system, and based on direct amperometric detection of NO with short response time (< 5 s) and sensitivity range 1 nM–20 μM. The analog signal was digitalized with a four-channel recording system and transferred to a computer. The sensor was accurately calibrated by mixing standard solutions of $NaNO_2$ with 0.1 M H_2SO_4 and 0.1 M KI according to the reaction:

$$4H^+ + 2I^- + 2NO_2^- \rightarrow 2H_2O + 2NO + I_2$$

Irradiation was performed in a thermostated quartz cell (1 cm path length, 3 mL capacity, 25°C) by using the monochromatic radiation at 420 nm of the Fluorolog-2 as the light source. NO measurements were carried out with the electrode positioned outside the light path in order to avoid NO signal artefacts due to photoelectric interference on the ISO-NO electrode.

Two-photon laser scanning fluorescence microscopy and spectroscopy. Two-photon fluorescence microscopy of **1** in the presence of **2** + **3** was performed using a LSM 710 NLO microscope (Carl Zeiss, Jena, Germany) equipped with mode-locked femtosecond pulsed

Mai Tai DeepSee laser tunable in the wavelength region 700 – 1100 nm, and Plan-Apochromat 20x water immersion objective (NA 1.0) (Carl Zeiss, Jena, Germany). Fluorescence was registered with descanned (internal) detectors with a fully opened pinhole. Emission spectra were acquired by using the spectral detector on the system, evaluating the grey value of the TPM images. The excitation wavelength was set to 840 nm. Laser power at the sample, was approximately 15 mW. Band pass filters, 600-760 nm and 470-570 nm, were used to record signals of the complete NPs and autofluorescence respectively. Images were acquired with a pixel dwell time of 1.58 µs. The image frame size was 1024 x 1024 pixels, which corresponds to a surface area of 425 x 425 µm. 3D imaging was performed by acquiring z-stacks of images at different sample depths. Image processing was performed with ZEN (Carl Zeiss, Jena, Germany).

Binding studies. Titration experiments with detection of fluorescence were performed at constant **2** and variable **1** concentrations (excitation wavelength of 575 nm, isosbestic point, $A_{575} \sim 0.1$). The best complexation model and the related association constants were determined by global analysis of multiwavelength data sets corresponding to twelve different mixtures in a completely numerical procedure, using the commercial SPECFIT/32 program, based on the publications of H. Gampp *et al.*[17] The analysis can be applied to any spectroscopic quantity that can be linearly related to concentration. Fluorescence data can be analysed provided inner filter distortions are negligible. Given the relation that must exist between the concentration of the various species in the postulated simultaneous equilibria, the program calculates the conditional association constants and the spectra of the complexes based on a multivariate optimization procedure based on Singular Value Decomposition (SVD) and non linear regression modelling by the Levenberg-Marquardt algorithm. The fits were evaluated on the basis of their Durbin-Watson (DW) factors and the relative error of fit. For further details on this application see for example ref. 23.

Cell viability studies. Human squamous carcinoma cells (A431, HPA cultures, Salisbury, UK) were maintained in phenol red-free minimum essential medium (MEM, Invitrogen, Pailsey, UK), supplemented with 10% fetal bovine serum (FBS), 2 mM glutamine EMEM,

1% non essential amino acids (NEAA) at 37°C and in a 5% CO_2 incubator. A431 cells were seeded into 96 well-plates in a concentration of 10^4 per well and allowed to grow for 24 h. Afterwards, the full-growth media was substituted with FBS-free media for control samples and FBS-free media including the tested compounds at a volume of 100 µL. Incubation time: 1 h. To evaluate the dark- and phototoxicity of the tested solutions, one plate was kept in dark and outside the incubator and the other plate was irradiated with LED array 1 (PAU62206 (#M10290), PAU62406 (#M9928), LATAB, Vällingby, Sweden). The setup allowed for simultaneous irradiation with 405 nm (±10 nm) and 633 (±10 nm). The total light dose was 20 J/cm^2 (10 J/cm^2 per lamp). After irradiation, tested solutions were substituted with full growth media and plates were placed in the incubator for 24 h. Afterwards, 20 µL of MTT in cell media (5 mg/mL) (Sigma-aldrich, Sweden) was added to each well. After 2 h of incubation, media was replaced with 100 µL of 0.01 M HCL in DMSO for dissolving purple MTT formazan. Absorbance was measured at 540 nm using SpectraMax M2 Multi-Mode Microplate Reader (Molecular Devices,USA).

Cell imaging studies. Prior to the microscopy experiments, 2×10^4 cells were seeded on 3 cm glass-bottom petri dish and left in the incubator for 24 h. The full growth media was substituted with a tested solution 1 h before imaging; Before imaging, tested solution was removed and cells carefully rinsed with PBS and kept in FBS-free media during microscopy experiments.

Skin sample preparation. Human skin specimens from caucasian females, collected as leftovers from breast reduction surgery were used in experiments. The specimens were cut into 1 x 1 cm pieces, stored in -70 ° C and used within six months. The samples were thawed in room temperature before use. A major part of subcutis was removed mechanically, using a scalpel. Afterwards, full-thickness skin samples were mounted in flow-through diffusion chambers, for exposure to the different test solutions. The receptor compartment was filled with PBS solution and the experimental solutions were added to the donor compartment. Diffusion chambers were covered with parafilm and aluminium foil and kept at 30 °C temperature. Passive diffusion was allowed for 20 hours under constant stirring of donor

compartment. After exposure, samples were taken out of the diffusion chamber, thoroughly rinsed with PBS solution and mounted on the microscopy slides using custom made imaging chambers consisting of a No. 1.5 cover slip (0.18 mm, Menzel-Gläser) and a double-sided sticky tape.

Results and Discussion

Design, self-assembly and spectroscopic properties. Polymer **1** consists of β-CD units interconnected by epichlorohydrin spacers to form glyceryl cross-linked β-CD polymer. This polymer is well tolerated *in vivo*[13c] and highly soluble in water where it exists under the form of nanoparticles (NPs) of *ca.* 25 nm in diameter.[13b,h] Due to the presence of different hydrophobic nanodomains these NPs are able to entrap a variety of guests[13i,14,15] with enhanced stability constants and payloads as compared with the unmodified β–CD.

The phthalocyanine **2** is a well-known red photoemitter, an effective $^1O_2$ photogenerator[18] and possess a large two-photon absorption cross section.[19] This photosensitizer is soluble in aqueous solution where it exhibits absorption bands with maxima at 335 and 635 nm, respectively. However, the formation of water soluble aggregates[20] makes **2** photodynamically inactive as demonstrated by the low fluorescence yield and lack of photogeneration of $^1O_2$. Addition of increasing amounts of the polymer **1** to the aqueous solution of **2** results in the dramatic modification on the absorption profile (Figure 1A). In particular, the intensity of the visible band at 635 nm reduces and is accompanied by a concomitant formation of a new absorption band at 680 nm as well as an increase of the UV band. In addition, a significant intensification of the characteristic red emission of **2** was observed (Figure 1B) upon increasing amount of the polymer **1**. This spectroscopic behaviour is in line with a significant de-aggregation and accounts for the encapsulation of **2** within the polymer NPs of **1**.[20] Mechanistically the compound **2** is able to interact with the β-CD units as the extended benzene ring can actively participate in the inclusion process.[21] On the basis of related studies of porphyrinoid derivatives, co-operative interactions induced by hydrophobic domain of folded polymer might enhance the internalization of **2** within **1**. To

gain insights into the interaction of **2** with the β-CD-based NPs, we analysed the fluorescence data by a global method (see Experimental Section), expressing the host concentration in β-CD units on basis of the known β-CD content of the polymer (70% w/w), according to an approach already applied.[22] We included in the analysis the dimerization equilibrium of **2** in water with constant log (K_d/M^{-1}) = 5.99 (fixed).[23] Only monomeric species were considered as being emissive. A model involving β-CD unit:**2** complexes with 1:1 and 1:2 stoichiometry was found to fairly reproduce the experimental data over the whole wavelength range 640-800 nm with equilibrium constants log (K_{11}/M^{-1}) = 3.52 ± 0.03 and log (K_{12}/M^{-2}) = 8.50 ± 0.23 (Durbin-Watson factor is 1.54 and relative error of fit is 3.39 %) (Figure 2A) The emitting species concentration as a function of the amount of polymer **1** is reported in Figure 2B. The global fitting calculation also afforded the fluorescence molar amplitudes for excitation at 575 nm of the two monomeric species of **2**, *i.e.*

the free molecule and the 1:1 complex (inset Figure 2A). The enhancement in the fluorescence amplitude of **2** bound to the polymer with the emission maximum undergoing bathochromic shift of *ca.* ~ 8 nm, reflects the expected environmental effects on the photophysical features of the photosensitizer **2**. This molecule is indeed characterized by stronger and red shifted emission in non aqueous media compared to phosphate buffer.[23] The high binding constant for 1:1 complexation makes the system to be monomerized at > 85% extent at the highest polymer concentration. This can be understood considering that the benzene sulfonate moieties attached on the macrocyclic structure of **2** are available to interact with the β-CD units due to their favourable geometrical matching. Entrapment of **2** as monomer can be favoured by the 3D frame of the CD polymer where the high local concentration of host units and the presence of nanocavities in the crosslinked network may concur to disrupt the dimer.

The photoactive compound **3** was designed to ensure its efficent encapsulation within the β-CD-based NPs. It integrates an adamantyl appendage and a commercially available nitroaniline derivative in the same covalent backbone. This nitroderivative is a suitable NO photodonor as it satisfies several prerequisites for bio-applications, including excitation with

visible light and formation of non-toxic side photoproducts.[24] The twisted conformation of the nitro group with respect to the aromatic plane is crucial for the NO photorelease. However, it has been shown that incorporation of this chromophore within a β-CD cavity leads to a partial planarization of the nitrogroup with consequent dramatic inhibition of the NO photoreleasing properties.[25] In this view, the presence of the adamantyl fragment in the structure of **3** was deliberately chosen to avoid this potential drawback. In fact, adamantane moiety is a well-known guest for β-CD since it fits inside the cavity[26] precluding, in principle, the incorporation of the NO photodonor therein. In fact, the binding constant of the adamantane moiety for unfunctionalized β-CD[26] is more than one order of magnitude larger than that of the nitroaniline chromophore.[25] Compound **3** is insoluble in aqueous solution. However, it becomes fairly soluble in the presence of the β-CD polymer **1** as indicated by the appearance of the characteristic absorption of the nitroaniline chromophore in the visible region (***a*** in Figure 3).

The spectrum of a mixture of the three components (**1** + **2** + **3**) reveals the absorption of both chromophores. The spectral characteristics observed (***c*** in Figure 3) match fairly well the profile obtained by summing the spectra of the NPs loaded with **2** or **3** separately (***a*** and ***b*** in Figure 3), and reveal the absence of strong interactions between the individual chromophores each other, in the ground state. Moreover, the unaltered position of the absorption maxima with respect to those observed for the separated chromophores indicates that their co-encapsulation does not induce any rearrangement (*i.e*. displacement/aggregation) of the individual chromogenic centres. This might be the consequence of a different affinity of the two components for the diverse binding sites of the NPs. Dynamic light scattering data (inset Figure 3) indicate the average hydrodynamic diameters of these supramolecular assemblies to be *ca.* 25 and 35 nm in the absence and presence of both guests, respectively. Guest association to the NP surface and structural rearrangements of the host-guest supramolecular system upon guest incorporation may contribute to increase the size of the loaded NPs.

Interestingly, the emission properties of **2** were not affected in the case of the bichromophoric nanoassembly (***d*** and ***e*** in Figure 3) ruling out any intramolecular quenching (*for example, by*

photoinduced electron transfer) of the excited phthalocyanine by the NO photodonor. The preservation of the fluorescence properties of the phthalocyanine under these experimental conditions is a crucial pre-requisite for detection in living cells.

TPE fluorescence microscopy and spectroscopy. Figure 4(A,B, and C) shows optical microscopy images of epidermal cancer A431 cells acquired after incubation with the polymer nanoassembly (**1** + **2** + **3**), acquired by registering the fluorescence of the phthalocyanine moiety using TPM. The images indicate that the nanoassembly partly accumulate at the cell surface or in the membrane; however a dominating part of the fluorescence is detected within the cytoplasm, implying that the polymer, not directly detectable by fluorescence, does not prevent the photosensitizer is taken up by the cells, which is crucial in order it can develop its phototherapeutic action (*vide infra*). The spectral characteristics of the photosensitizer were also assessed in A431 cells. The spectral profile of the TPE red fluorescence arising within the biological system was basically identical with the emission of the pure nanoassembly dispersed in aqueous medium (Figure 4D). This fact points to the penetration of the nanoassembly as such across the cell membrane. The seemingly small shift in emission maxima observed is most likely caused by the coarse spectral resolution (~10 nm) of the spectral detector on the TPM set up and cannot be regarded as significant.

To investigate the potential of the nanoassembly to deliver the photosensitizer to tissue, the same bichromophoric nanoconstruct was applied topically to human skin *ex vivo*. Figure 4E-H reveals the fluorescence distribution pattern after 24 hours of application to human skin detected by TPM. As shown by the images, the photosensitizer have a extracellular uptake route in the upper epidermal layers down to depths of 15 μm, visualized as bright fluorescence in the extracellular space, while the dark regions are present within the cells (Figure 4F,G). The penetration pattern is similar to that observed for other compounds delivered to human skin in solution.[27] Deeper into the tissue, fluorescence was mainly found to localize within skin fissures and wrinkles (Figure 4H) and detected down to depths more than 25 μm (data not shown). The presence of the nanoassembly within the fissures serves as

a reservoir allowing for diffusion into epithelium in agreement with studies of other compounds.[27]

Photodynamic properties. The excited triplet state of the phthalocyanines is the key transient intermediate for the photosensitization of $^1O_2$ and its effective generation is thus crucial for the photodynamic action.[4] Laser excitation of compound **2** in phosphate buffer solution in the absence of the polymer **1** does not lead to negligible transient signal, according with the effective aggregation which precludes the triplet population. In contrast, encapsulation of **2** within the NPs results in the formation of the typical triplet-triplet transient absorption with maximum at *ca.* 500 nm (Figure 5A) decaying in the hundreds of microsecond time regime (Inset Figure 5A).[28] This transient was effectively quenched by oxygen with a bimolecular quenching constant of *ca.* $0.8x10^9$ M^{-1} s^{-1}. Analogously to what observed for the fluorescence emission, co-encapsulation of **2** and **3** within the polymer NPs of **1** does not change significantly the efficiency of the triplet population. In fact, since the two samples were optically matched at the excitation wavelength, the intensity of the transient absorption is directly related to the triplet quantum yield (Figure 5A). Energy transfer from the triplet of **2** to molecular oxygen results in the photogeneration of $^1O_2$ as directly proven by its typical phosphorescence signal at 1270 nm decaying with a first-order kinetic in *ca.* 3.6 μs (Figure 5B).[29]

The NO photorelease properties of the complete polymeric nanoassembly were demonstrated by the direct and real-time monitoring of this transient species using an ultrasensitive NO electrode which directly detects NO with nM concentration sensitivity by an amperometric technique.[30] The results illustrated in Figure 6A provide evidence that the nanoassembly is stable in the dark but supplies NO exclusively upon illumination with visible light. Figure 6B shows the changes in the electronic absorption spectrum of the bichromophoric polymeric NPs observed upon irradiation. The spectral evolution with illumination time shows a bleaching occurring around 400 nm. These spectral features account for a photochemical reaction involving exclusively the photoactive compound **3**, being in excellent agreement with the photochemical pathway leading to NO release previously proposed for the single NO

photodonor unit.[24] Accordingly, no significant changes are observed beyond 500 nm, where the absorption is exclusively dominated by the phthalocyanine guest. That the phthalocyanine **2** is not involved in any photochemical process under photoexcitation of **3** was also confirmed by the almost complete preservation of the fluorescence spectrum observed after the photolysis experiments (Inset Figure 6B). Interestingly, the efficiency of the NO photorelease was the same as that observed when the polymer NPs of **1** were loaded only with **3** in the absence of **2** (data not shown). This rules out any potential energy transfer quenching process between **2** and **3** when co-encapsulated in the same host. Since a fluorescence resonance energy transfer type mechanism (occurring through space) is out of question due to the non emissive properties of component **3**, the lack of quenching observed rules out any significant physical contact between the two chromogenic centers within the lifetime of the excited state of **3**, probably as a result of their localization in different compartments of the polymer NPs. Moreover, the NO photorelease as well as the spectral evolution profile observed provide clear evidences that, according to the design of the nanoassembly, the nitroaniline chromophore is not included within the β-CD cavity of the polymer. If this would be the case, inhibition of the NO photoreleasing properties and different spectral changes upon light irradiation would have been produced.[25]

Photoinduced cell mortality. To validate the feasibility of using this nanoassembly for bimodal phototherapeutic activity, A431 human squamous carcinoma cells were incubated with the NPs and either kept in the dark or irradiated simulataneiously with 405 nm and 633 nm light, targeting the NO-photodonor **3** and phtalocyanine **2**, respectively. The results illustrated in Figure 7 show that the samples displayed a low dark cytotoxicity, accounting for a good biocompatibility of the NPs. Considerable cell mortality was observed after illumination when the NPs were loaded with either **2** or **3**. As demonstrated by the figure the photodynamic inactivation induced by the polymer NPs containing both the photoactive components (**2** and **3)** was significantly more pronounced compared to the effect observed with the NPs loaded with the single components, *i.e.* **2** or **3.** This finding provides evidence for a bimodal photo-inactivation

mechanism in neoplastic destruction using this nanoassembly, in which the simultaneous release of cytotoxic NO and $^1O_2$ is envisaged to play a key role.

Conclusion

Our results demonstrate that water soluble, biocompatible CD-based NPs with a multifunctional cargo can be obtained by co-entrapping of two distinct photoresponsive guests with a CD-based polymer. The different entrapped species can be operated independently under the exclusive control of light inputs, as proven by the preservation of their photochemical and photophysical properties. One photoresponsive guest exhibits red fluorescence and generation of the cytotoxic species $^1O_2$ upon irradiation, while the other permits the generation of NO. It should be noted that in contrast to non-photoresponsive compounds, the preservation of the photobehavior of independent components after their confinement in a restricted region of space is a "non-trivial" result. In most cases, the response to light of multiple photoactive units can in fact be considerably influenced, in both nature and efficiency, by the occurrence of competitive photoprocesses (*i.e.*, photoinduced energy and/or electron transfer, non-radiative deactivation, *etc.*), which preclude the final goal.[31] It has demonstrated here that the macromolecular host does not prevent crossing of the membrane of epidermal carcinoma cells by the photosensitizers, and likely transports itself its photoresponsive cargo within the cytoplasm as visualized by TPM. Furthermore, the nanoassembly can be delivered to tissue, here exemplified by *ex vivo* exposure experiments to human skin performed in this study. By using TPM, the fluorescence results using NPs loaded with the photoresponsive guests demonstrate they are able to diffuse into the epidermis of the skin together with their cargo of active molecules. Furthermore, the simultaneous photogeneration of the cytotoxic species $^1O_2$ and NO, results in an amplified cell photomortality most likely due to a combined effect. The convergence of dual therapeutic photodynamic action and TPE imaging capability in a single nanostructure together with its biocompatibility make the present CD-based nanoassembly an appealing candidate for further studies in biomedical research.

Acknowledgements

We thank the Marie Curie Program # 237962 CYCLON (FP7-PEOPLE-ITN-2008) for financial support to MC fellows VK and NK, and funding of the research. We acknowledge CCI, University of Gothenburg, for use of equipment and kind support from staff, and SkinResQU for access to cell culturing facilities. We also thank the MIUR (PRIN 2011) for financial support.

References

(1) Lane, D; *Nat. Biotech*. **2006**, *24*, 163-164.

(2) (a) Sortino, S. *J. Mater. Chem*. **2012**, *22*, 301-318; (b) Yan, B.; Boyer, J. C.; Branda, N. R.; Zhao, Y. *J. Am. Chem. Soc*. **2011**, *133*, 19714-19717; (c) Brieke, C.; Rohrbach, F.; Gottschalk, A.; Mayer G.; Heckel, A. *Angew. Chem. Int. Ed*. **2012**, 51, 8446-8476; (d) Rai, P.; Mallidi, S.; Zheng, X.; Rahmanzadeh, R.; Mir, Y.; Elrington, S.; Khurshid, A.; Hasan, T. *Adv. Drug. Delivery Rev*. **2010**, *62*, 1094-1124; (e) Shao, Q.; Xing, B. *Chem. Soc. Rev*. **2010**, *39*, 2835-2846; (f) Sortino, S. *Photochem. Photobiol. Sci*. **2008**, *7*, 911-924.

(3) See, for example: (a) Bhattacharya, R.; Mukherjee, P. A*dv. Drug Delivery Rev.,* **2008**, *60*, 1289-1306; (b) Jang, B.; Park, J.-Y.; Tung, C.-H.; Kim, I.-H.; Choi, Y. *ACS Nano,* **2011**, *5*, 1086-1094; (c) Stephanopoulos, N.; Tong, G. J.; Hsiao, S. C.; Francis, M. B. *ACS Nano,* **2010**, *4*, 6014-6020; (d) Brown, P. K.; Qureshi, A. T.; Moll, A. N.; Hayes, D. J.; Monroe, W. T. *ACS Nano*, **2013**, *7*, 4, 2948-2959; (e) Mazzaglia, A.; Sciortino, M. T.; Kandoth, N.; Sortino, S. *J. Drug Deliv. Sci. Tech.* **2012**, *22*, 3, 235-242.

(4) (a) Castano, A. P.; Mroz, P.; Hamblin, M. R. *Nat. Rev. Cancer* **2006**, *6*, 535-545; (b) Celli, J. P.; Spring, B. Q.; Rizvi, I.; Evans, C. L.; Samkoe, K. S.; Verma, S.; Pogue, B. W.; Hasan, T. *Chem. Rev*. **2010**, *12*, 2795-2838; (c) Master, A.; Livingston M.; Sen Gupta A. *J. Control. Release*, **2013**, *168*, 1, 88-102; (d) Pandey, R.; Zheng, G.; In *The Porphyrin Handbook*; Smith, K. M.; Kadish, K.; Guilard, R.; Eds.; Academic Press: San Diego, **2000**; Vol. 6. pp. 157-230.

(5) (a) Sortino, S. *Chem. Soc. Rev.* **2010***, 39,* 2903-2913; (b) Fraix, A.; Kandoth, N.; Sortino, S.; *In Specialist Periodical Reports in Photochemistry*, **2013**, vol. 41, 302-318; (c) Ford, P. C. *Nitric Oxide* **2013**, *34*, 56–64.

(6) (a) *Nitric Oxide: Biology and Pathobiology*, Ed. Ignarro, L. J. Elsevier Inc., **2010**; (b) Special Journal Issue on Nitric Oxide Chemistry and Biology. Ed. Ignarro, L. J. *Arch. Pharmacal Res*. **2009.**

(7) (a) Fukumura, D.; Kashiwagi, S.; Jain, R. K. *Nat. Rev. Cancer* **2006**, *6*, 521-534; (b) Xu, W.; Liu, L. Z.; Loizidou, M.; Ahmed, M.; Charles, I. G. *Cell. Res.* **2002**, *12*, 311-320; *Nitric Oxide Donors for Pharmaceutical and Biological Applications*. Eds. Wang, P. G.; Cai, T. B.; N. Taniguchi, **2005**, Wiley-VCH Verlag GmbH & Co. KGaA, Weinheim, Germany; (c) P. C. Ford, *Acc. Chem. Res*. **2008**, *41*, 190; (d) Fry, N. L.; Mascharak, P. K. *Acc. Chem. Res*. **2011**, *44*, 289-298; (e) Ostrowski, A. D.; Ford, P. C. *Dalton Trans*. **2009**, 10660-10669; (f) Carpenter, A. W.; Schoenfisch, M. H. *Chem. Soc. Rev*. **2012**, *41*, 3742-3752.

(8) Prasad, P. N. *Introduction to Biophotonics*; Wiley: New York, **2003**; (b) Wang, F. F; Yang, X. J.; Ma, L.; Huang B. R.; Na, N.; He, Y. C. E, D. C.; Ouyang, J. *J. Mater. Chem.*, **2012**, *22*, 24597-24604; (c) Zipfel, W. R.; Williams, R. M.; Webb, W. W. *Nat. Biotech*. **2003**, *21*, 1368-1376.

(9) (a) Kataoka, K.; Kwon, G. S.; Yokoyama, M.; Okano T.; Sakurai, Y. *J. Control. Release* **1993**, *24*, 119–132; (b) Torchilin, V. P. *J. Control. Release* **2001**, *73*, 137–172; (c) Husseini A. G.; Pitt, W. G. *Adv. Drug Deliv. Rev.* **2008**, *60*, 1137–1152; (d) Park, J. H.; Lee, S.; Kim, J. H.; Park, K.; Kim K.; Kwon, I. C. *Prog. Polym. Sci.* **2008**, *33*, 113–137; (e) Kim, S.; Shi, Y.; Kim, J. Y.; Park, K.; Cheng, J.-X. *Expert Opin. Drug Deliv.* **2010**, 7, 49–62.

(10) Swaminathan, S.; Garcia-Amorós, J.; Fraix, A.; Kandoth, N.; Sortino S.; Raymo, F. M. *Chem. Soc. Rev.* **2014**; DOI:10.1039/c3cs60324e.

(11) (a) O'Reilly, R. K.; Hawker C. J.; Wooley, K. L. *Chem. Soc. Rev.* **2006**, *35*, 1068−1083; (b) Zhao, Y. *Chem. Rec.* **2007**, 7, 286–294; (c) Y. Zhao, *J. Mater. Chem.* **2009**, *19*, 4887–4895; (d) Zhao, Y. *Macromolecules*, **2012**, *45*, 3647−3657; (e) Gohy

J.-F.; Zhao, Y. *Chem. Soc. Rev.* **2013**, *42*, 7117-7129; (e) Esser-Kahn, A. P.; Odom, S. A.; Sottos, N. R.; White S. R.; Moore, J. S.; *Macromolecules* **2011**, *44*, 5539–5553.

(12) (a) Ma, N.; Wang, Y.; Wang, Z.; Zhang, X. *Langmuir* **2006**, *22*, 3906–3909; (b) Harbron, E. J.; Davis, C. M.; Campbell, J. K.; Allred, R. M.; Kovary M. T.; Economou, N. J. *J. Phys. Chem. C* **2009**, *113,* 13707–13714; (c) Davis, C. M.; Childress E. S.; Harbron, E. J. *J. Phys. Chem. C* **2011**, *115*, 19065–19073; (d) Yildiz, I., Impellizzeri, S.; Deniz, E.; McCaughan, B.; Callan J. F.; Raymo, F. M.; *J. Am. Chem. Soc.* **2011**, *133*, 871–879; (e) Deniz, E.; Tomasulo, M.; Cusido, J.; Sortino, S.; Raymo, F. M. *Langmuir* **2011**, *27*, 11773–11783; (f) Deniz, E.; Tomasulo, M.; Cusido, J.; I. Yildiz, Petriella, M.; Bossi, M. L.; Sortino, S.; Raymo, F. M. *J. Phys. Chem. C* **2012**, *116*, 6058−6068; (g) Cusido, J.; Battal, M.; Deniz, E.; Yildiz, I.; Sortino, S.; Raymo, F. M. *Chem. Eur. J.* **2012**, *18*, 10399–10407; (h) Raymo, F. M. *J. Phys. Chem. Lett.* **2012**, *3*, 2379–2385; (i) Raymo, F. M. *Isr. J. Chem.* **2013**, *53*, 247–255.

(13) (a) Renard, E.; Deratani, A.; Volet, G.; Sebille, B. *Eur. Polym. J.*, **1997**, *33*, 49-57; (b) Othman, M.; Bouchemal, K.; Couvreur, P.; Desmaële, D.; Morvan, E.; Pouget T.; Gref, R. *J. Colloid Interface Sci.* **2011**, *354*, 517-527; (c) Daoud-Mahammed, S.; Grossiord, J. L.; Bergua, T.; Amiel, C.; Couvreur P.; Gref, R. *J. Biomed. Mater. Res. A* **2008**, *86*, 736-748; (d) Daoud-Mahammed, S.; Couvreur, P.; Amiel, C.; Besnard, M.; Appel M.; Gref, R. *J. Drug Deliv. Sci. Technol.* **2004**, *14*, 51-55; (e) Daoud-Mahammed, S.; Ringard-Lefebvre, C.; Razzouq, N.; Rosilio, V.; Gillet, B.; Couvreur, P.; Amiel, C.; Gref, R. *J. Colloid Interface Sci.* **2007**, *307*, 83-93; (f) Daoud-Mahammed, S.; Couvreur, P.; Gref, R. *Int. J. Pharm.* **2007**, *332*, 185-191; (g) Gref, R.; Amiel, C.; Molinard, K.; Daoud-Mahammed, S.; Sebille, B.; Gillet, B.; Beloeil, J. C.; Ringard, C.; Rosilio, V.; Poupaert, J.; Couvreur, P. *J. Control. Release* **2006**, *111*, 316-324; (h) Daoud-Mahammed, S.; Couvreur, P.; Bouchemal, K.; Cheron, M.; Lebas, G.; Amiel, C.; Gref, R. *Biomacromolecules* **2009**, *10*, 547-554; (i) Battistini, E.; Gianolio, E.; Gref, R.; Couvreur, P.; Fuzerova, S.; Othman, M.; Aime, S.; Badet, B.; Durand, P.; *Chem. Eur. J.* **2008**, *14*, 4551–4561 (l) Gidwani, B.; Vyas, A.; *Colloids Surf B Biointerfaces* **2014**, *114*, 130-137.

(14) Anand, R.; Manoli, F.; Manet, I.; Daoud-Mahammed, S.; Agostoni, V.; Gref, R.; Monti, S. *Photochem. Photobiol. Sci.* **2012**, *11*, 1285-1292.

(15) (a) Fraix, A.; Kandoth, N.; Manet, I.; Cardile, V.; Graziano, A. C. E.; Gref, R.; Sortino, S. *Chem. Commun.* **2013**, *49*, 4459-4461; (b) Deniz, E.; Kandoth, N.; Fraix, A.; Cardile, V.; Graziano, A. C. E.; Lo Furno, D.; Gref, R.; Raymo, F. M.; Sortino, S. *Chem. Eur. J.* **2012**, *18*, 15782-15787.

(16) Kandoth, N.; Vittorino, E.; Sciortino, M. T.; Colao, I.; Mazzaglia, A.; Sortino, S.; *Chem. Eur. J.* **2012**, *18*, 1684-1690.

(17) (a) Gampp, H.; Maeder, M.; Meyer, C. J.; Zuberbühler, A. D.; *Talanta* **1985**, *32*, 95-101; (b) Gampp, H.; Maeder, M.; Meyer, C. J.; Zuberbühler, A. D. *Talanta* **1985**, *32*, 257-264.

(18) Karl, D.; Kadish, M.; Smith, K. M.; Guilard, R. In the Porphyrin Handbook, *Phthalocyanines: Properties and Materials* **2003**, Vol. 11-20, pp 168-170.

(19) Mir, Y.; van Lier, J. E.; Allard, J-F.; Morris, D.; Houd, D. *Photochem. Photobiol. Sci.* **2009**, *8,* 391-395.

(20) (a) Howe, L.; Zhang, J. Z. *J. Phys. Chem. A,* **1997**, *101,* 3207-3213; (b) M. Morisue, S. Ueda, Kurasawa, M.; Naito, M.; Kuroda, Y.; *J. Phys. Chem. A* **2012**, *116*, 5139−5144; (c) Ogunsipe, A.; Chenb, J. –Y.; Nyokong, T. *New. J. Chem*. **2004**, *28*, 822–827.

(21) (a) Park, J. W.; Song, H. J.; *J. Phys. Chem.* **1989**, *93,* 6454-6458; (b) Ruebner, A.; Yang, Z.; Leung, D.; Breslow, R. *Proc. Natl. Acad. Sci. USA* **1999**, *96*, 26, 14692–14693.

(22) Anand, R.; Manoli, F.; Manet, I.; -Mahammed, S. D.; Agostoni, V.; Gref, R.; Monti, S. *Photochem. Photobiol. Sci*. **2012**, *11*, 1285-1292.

(23) Brozek-Płuska, B.; Jarota, A.; Kurczewski, K.; Abramczyk, H. *J. Mol. Struct.* **2009**, *924–926*, 338–346

(24) (a) Caruso, E. B.; Petralia, S.; Conoci, S.; Giuffrida, S.; Sortino, S. *J. Am. Chem. Soc*. **2007**, *129*, 480-481; (b) Conoci, S.; Petralia S.; Sortino, S. **2006**, *EP2051935A1/US20090191284.*

(25) Sortino, S.; Giuffrida, S.; De Guidi, G.; Chillemi, R.; Petralia, S.; Marconi, G.; Condorelli, G.; Sciuto, S. *Photochem. Photobiol.* **2001**, *73*, 6-13.

(26) Rekharsky, M.; Inoue, Y. *Chem. Rev.* **1998**, *98*, 1875-1918.

(27) Bender, J.; Simonsson, C.; Smedh, M.; Engström, S.; Ericson, M. B. *J. Control. Release*, **2008**, *129*, 163-169.

(28) Montalti, M.; Credi, A.; Prodi, L.; Gandolfi, M. T. *Handbook of Photochemistry*, 3rd ed., CRC Press, Boca Raton, **2006**.

(29) Wilkinson, F.; Helman, W. P.; Ross, A. B. *J. Phys. Chem. Ref. Data* **1993**, *22*, 113–262.

(30) Coneski, P. N.; Schoenfisch, M. H.; *Chem. Soc. Rev.* **2012**, *41*, 3753-3758.

(31) (a) Ramamurthy, V. *Photochemistry in Organized and Constrained Media*, VCH, New York, **1991**; (b) Monti, S.; Sortino, S. *Chem. Soc. Rev.* **2002**, *31*, 287–300.

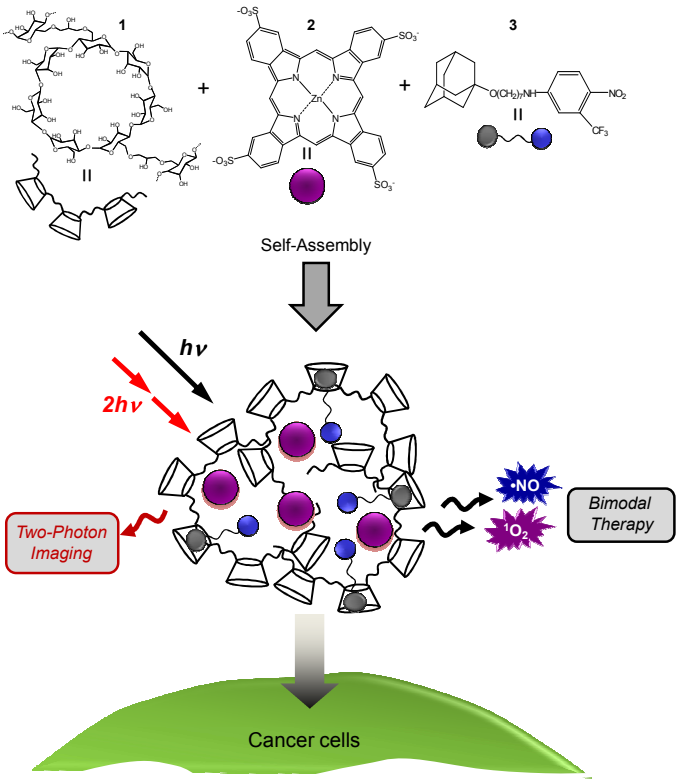

Scheme 1. Schematic illustration of the self-assebling photoresponsive polymer nanoparticles comprising: poly-β-cyclodextrin **1** as carrier, zinc phthalocyaninetetrasulfonate **2** acting as $^1O_2$ generating photosensitizer and red fluorophore, and an adamantyl-nitroaniline derivative **3** acting as NO photodonor.

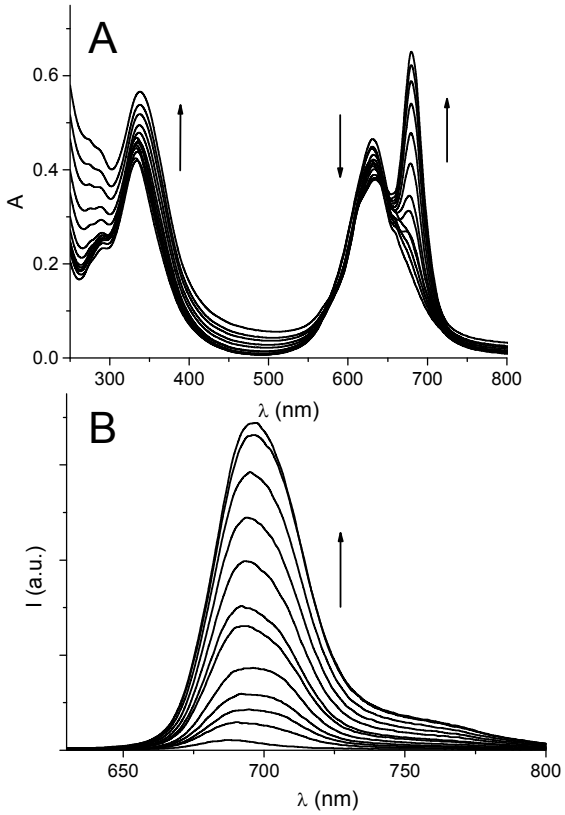

Figure 1. (**A**) Absorption and (**B**) fluorescence intensity changes observed for an aqueous solution (phosphate buffer 10 mM, pH = 7.4, 25°C) of **2** (15 μM) upon addition of increasing amounts of the polymer **1** in the range 0-7.75 mM (in β-CD units). λ_{exc} = 575 (isosbestic point).

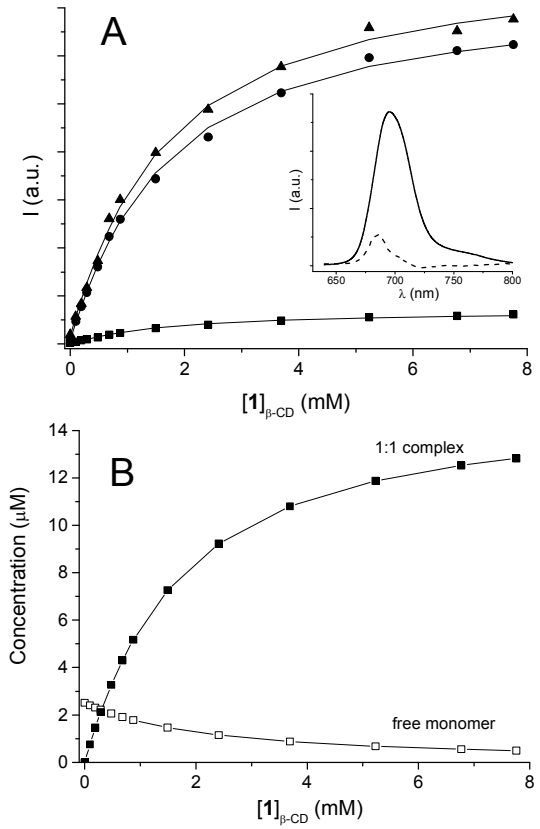

Figure 2. (**A**) Calculated (line) and experimental (symbol) emission intensities of **2** titrated with **1** at selected wavelengths: (▲) 693 nm (●) 704 nm, (■) 760 nm. The inset shows the calculated emission molar amplitudes of **2**, free monomer (dotted line) and 1:1 complex (solid line) with equilibrium constants given in the text. (**B**) The emitting species concentration as a function of the amount of polymer **1**.

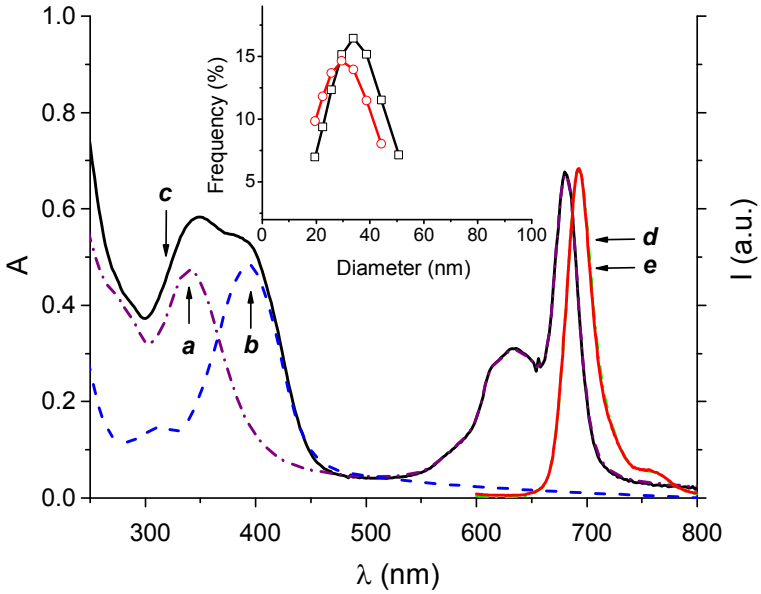

Figure 3. Absorption spectra of aqueous dispersions of **1** in the presence of **2** (***a***), **3** (***b***), and **2**+**3** (***c***). Fluorescence spectra of aqueous dispersions of **1** in the presence of **2** (***d***) and **2** + **3** (***e***), recorded at λ_{exc} = 575. The inset shows the hydrodynamic diameter for aqueous dispersion of **1** in the absence (○) and in the presence (□) of **2** + **3**. [**1**] = 11 μM (7.75 mM in β-CD); [**2**] = 15 μM; [**3**] = 40 μM. (Phosphate buffer 10 mM, pH 7.4, 25°C).

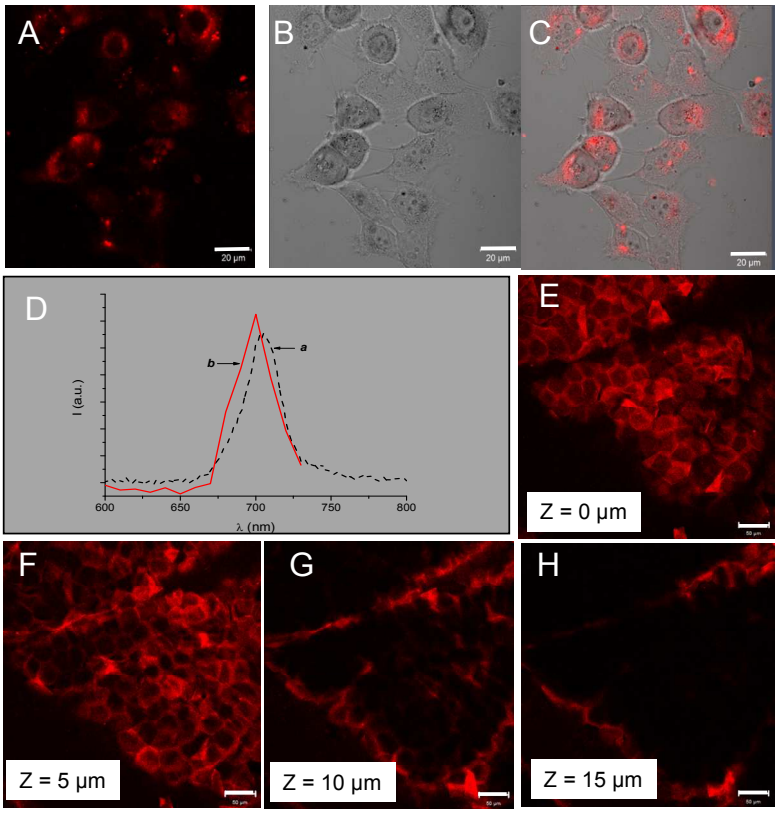

Figure 4. (**A**) TPE fluorescence microscopy (λ_{exc} = 840 nm), (**B**) transmission microscopy and (**C**) overlaid images of A431 human squamous carcinoma cells incubated with an aqueous dispersion of **1** in the presence of **2**+**3** (scale bar = 20 µm). (**D**) TPE fluorescence spectra of **1** in the presence of **2**+**3** (***a***) in the aqueous suspension of the polymer nanoassembly and (***b***) within A431 human squamous carcinoma cells upon incubation of the cell culture with the polymer nanoassembly. (**E-H**) Penetration depth and distribution pattern of an aqueous dispersion of **1** in the presence of **2**+**3** in human *ex-vivo* skin sample after 24 h of incubation in the flow through diffusion chamber (scale bar = 50 µm; λ_{exc} = 840 nm); Z represents the depth of the sample. In all these experiments [**1**] = 11 µM (7.75 mM in β-CD); [**2**] = 15 µM; [**3**] = 40 µM.

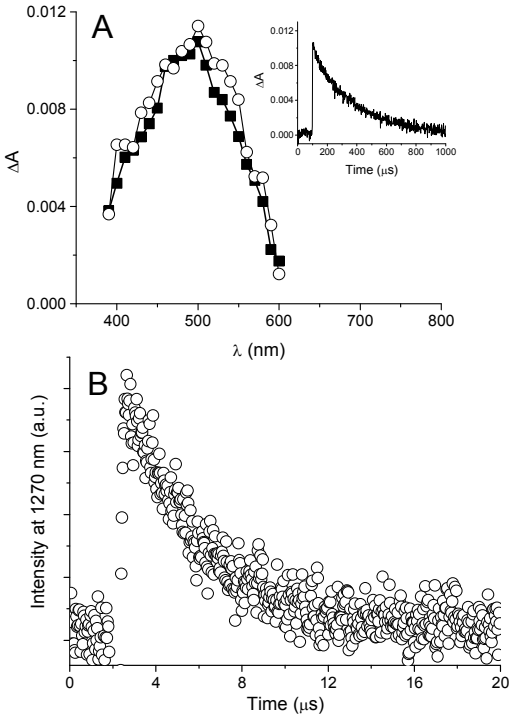

Figure 5. (**A**) Transient absorption spectra (λ_{exc} = 532 nm, E_{532} ~ 12 mJ/pulse, Ar saturated solution) of aqueous dispersion of **1** in the presence of **2** (○) and **2**+**3** (■). The inset shows the decay trace monitored at 500 nm (**B**) Representative decay kinetic of $^1O_2$ observed upon 532 nm laser excitation of aqueous dispersion of **1** in the presence of **2** + **3**. [**1**] = 11 μM (7.75 mM in β-CD); [**2**] = 15 μM; [**3**] = 40 μM. (Phosphate buffer 10 mM, pH 7.4, 25°C).

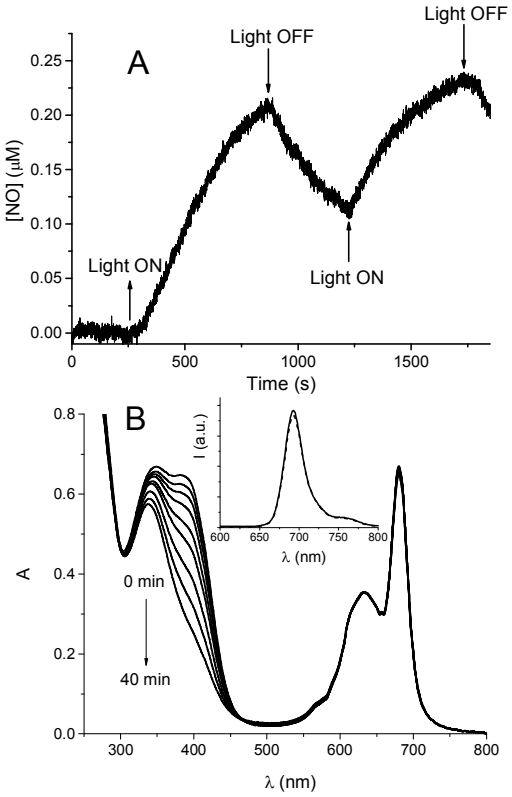

Figure 6. (**A**) NO release profile and (**B**) absorption spectral changes observed upon irradiation (λ_{exc} = 420 nm) of aqueous dispersion of **1** in the presence of **2**+**3**. The inset shows the fluorescence observed before (solid line) and after (dotted line) the photolysis. [**1**] = 11 μM (7.75 mM in β-CD); [**2**] = 15 μM; [**3**] = 40 μM. (Phosphate buffer 10 mM, pH 7.4, 25°C).

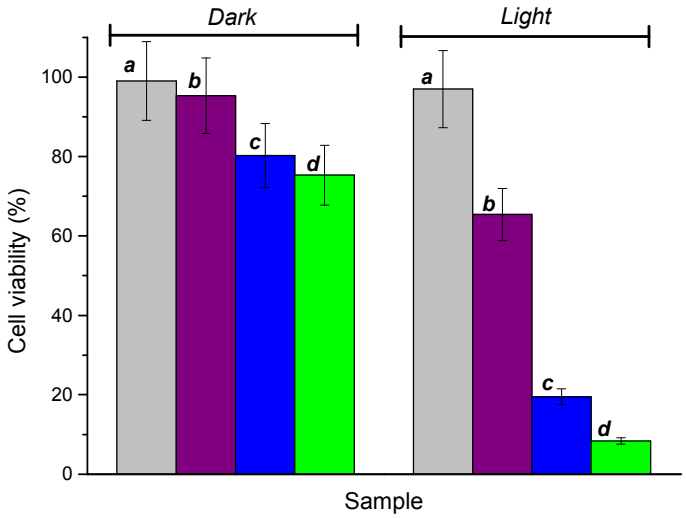

Figure 7. Dark and photoinduced mortality of A431 human squamous carcinoma cells incubated with aqueous dispersion of **1** in the absence (***a***) and in the presence of **2** (***b***)**, 3** (***c***) and **2**+**3** (***d***)**.** The samples were simultaneously irradiated with 405 nm (10 J/cm^2) and 633 nm (10 J/cm^2) LED sources. [**1**] = 11 μM (7.75 mM in β-CD); [**2**] = 15 μM; [**3**] = 40 μM.

TOC

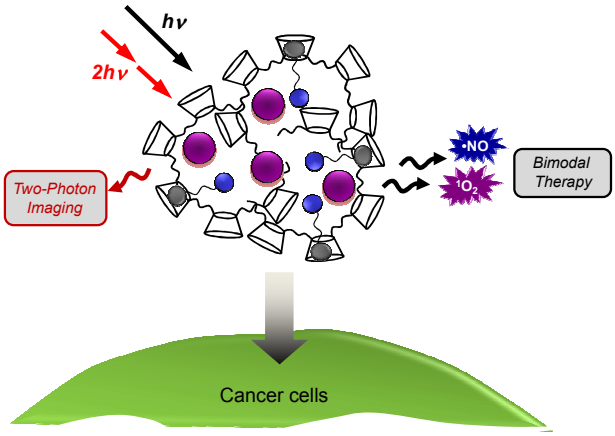
hν
2hν
Two-Photon Imaging
•NO
$^1O_2$
Bimodal Therapy
Cancer cells